Article

Comparison of Pressure Pulsation Characteristics of Francis Turbine with Different Draft Tube Arrangement Direction

Tao Zhang [1], Zilong Hu [2], Xinjun Liu [3], Jiahao Lu [2], Xijie Song [4], Di Zhu [5] and Zhengwei Wang [4,*]

1   Technical Management Department, Y. R. Wanjiazhai Water Multi-Purpose Dam Project Co., Ltd., Taiyuan 030000, China; 15047748589@163.com
2   College of Water Resources and Civil Engineering, China Agricultural University, Beijing 100083, China; huzilong1999@cau.edu.cn (Z.H.); lujiahao2209@cau.edu.cn (J.L.)
3   Power Station Management Bureau, Y. R. Wanjiazhai Water Multi-Purpose Dam Project Co., Ltd., Taiyuan 030000, China; hwgslxj_wjz@163.com
4   State Key Laboratory of Hydroscience and Engineering, Department of Energy and Power Engineering, Tsinghua University, Beijing 100084, China; songxijie@mail.tsinghua.edu.cn
5   College of Engineering, China Agricultural University, Beijing 100083, China; zhu_di@cau.edu.cn
*   Correspondence: wzw@mail.tsinghua.edu.cn

Abstract: Hydroelectric power generation is an important clean energy source, and the stability of water turbine operation determines the quality of hydro energy utilization. For hydro turbines, the layout direction of the draft tube is often only considered from a structural perspective, ignoring the hydrodynamic characteristics. This study adopts the computational fluid dynamics method and verifies the effectiveness of numerical simulation with experimental results, analyzing the influence of asymmetric draft tube layout direction on pressure pulsation of mixed flow turbine. The results show that under different working conditions, there is basically no difference in efficiency corresponding to different inclined directions of the draft tube, and the relative difference in performance values is less than 1%. From the perspective of internal flow, the working condition has a greater impact on the flow, and the draft tube tilt has a smaller impact. Under strong swirling flow conditions in the draft tube, the variational mode decomposition of pressure fluctuation is carried out. Research has found 7 characteristic frequency bands including 140 Hz, 80–90 Hz, 40–46 Hz, 5.5–6.5 Hz, 2.5–3 Hz, 1.67 Hz, and <1 Hz. The frequency of the dominant mode corresponding to the left tilt is higher, while the amplitude of the runner frequency is slightly lower. In general, left tilt is not only more suitable for unit layout but also has a better effect on draft tube pressure fluctuation, which is worthy of application in engineering.

Keywords: Francis turbine; pressure pulsation; draft tube design; hydrodynamic analysis; variational mode decomposition

1. Introduction

The excessive use of fossil energy has led to the emission of a large number of greenhouse gases, the rise of global temperature, the melting of glaciers, and the rise of sea level. In order to alleviate this dilemma and reduce the need for fossil energy, we have been looking for a new type of sustainable, renewable, and efficient energy. Studies have shown that with the development of renewable energy technology, the use of fossil energy as the main energy source has seen a huge decline in the past decade, and new renewable energy, such as hydro energy [1], wind energy [2], marine energy [3], and solar energy [4], has gradually occupied a dominant position in the energy structure. The carbon reduction of conventional energy-consuming machinery has also become a key research object [5–7]. Among all the energies, hydropower is a type of clean energy and occupies the largest proportion of renewable energy [8]. Francis turbine plays a vital role as an important component of hydropower generation [9]. It converts the gravitational potential energy of

the water flow into fluid kinetic energy, which drives the rotor to generate electricity. In recent years, due to the development of other energy technologies, such as wind energy and photovoltaics, the randomness of these energy sources makes the turbine operate under off-design conditions to meet the requirements of a stable grid [10]. However, due to the inherent performance of the Francis turbine, when the runner runs under off-design conditions, the increase or decrease in the runner's flow will exert a rotational component on the flow in the runner, resulting in the formation of flow gaps in draft tube, and flow gaps cause reflux in draft tube [11,12]. The reflux further develops into the vortex and the subsequent pressure pulsation. The generation of pressure pulsation will reduce the operation efficiency of the unit, causing vibration and noise in the operation of the unit [13,14]. Excessive pressure pulsations will reduce the operation life of the unit and even induce serious engineering accidents [15,16]. So for the Francis turbine draft tube, a pressure pulsation study is very necessary.

The draft tube plays a very important role as one of the components of the Francis turbine. The draft tube is located below the runner, and the fluid in the draft tube undergoes energy conversion from fluid kinetic energy to static pressure. Approximately 80% of energy conversion occurs in the draft tube cone, which is approximately 10% of the total length of the draft tube cone. The flow field of the draft tube can vary with different operating conditions [17,18]. For the Francis turbine, we can change the unit operating flow by controlling the opening of the movable guide vane. Due to changes in flow conditions, a vortex rope of the draft tube is formed. A large number of researchers have conducted a lot of studies on the formation of vortex ropes of the draft tube. Liu et al. [19] conducted a comprehensive and in-depth analysis of the unsteady turbulence and pressure pulsation of the Three Gorges hydroelectric unit, demonstrating the low-frequency characteristics of vortex rope pulsation. Liao et al. [20], based on unsteady calculation, determined typical locations where low-frequency pulsations are concentrated, such as the elbow section of the draft tube. Zhang et al. [21] revealed the spatial asymmetry of pressure pulsation distribution in draft tube vortex belts through numerical simulation. The numerical study of Pasche et al. [22] shows that the vortex rope and the draft tube wall are coupled, resulting in the pressure pulsation being transformed into the violent vibration of the unit structure. Existing research has shown that the phenomenon of pressure pulsation is extremely complex and may exhibit significant differences when slightly affected. The issue of the layout direction of the draft tube of the hydraulic turbine was originally a slight geometric difference, but it may cause a change in pressure pulsation. However, there is still a lack of research and clear conclusions.

By analyzing the draft tube pressure pulsation signal, we can find out the cause of draft tube pressure pulsation. A large number of scholars have used fast Fourier transform (FFT) to study the decomposition of pressure pulsation signals, and FFT has certain advantages in the convenience of signal decomposition. Jin et al. [23] conducted a fast Fourier transform analysis of the leakage flow in the Kaplan turbine, focusing on the impact of the flow of the tip gap on turbine performance and hydraulic efficiency. Wu et al. [24] compared the DMD method with the FFT method and retrograde method for the dynamic pattern structure analysis of the Savonius turbine near the wake region, providing a new idea for flow state analysis. Tian et al. [25] improved the traditional FFT and proposed that ZOOM-FFT can effectively diagnose and analyze the fault of submersible sewage pumps, aiming at the operation of mixed-flow pumps as turbines. Wang et al. [26] studied the pressure pulsation at the inlet of the volute, the second section of the volute, and the draft tube under out-of-control conditions of turbine runaway and analyzed the frequency domain characteristics of the pressure pulsation based on FFT. Tang [27] used adaptive noise complete geometric empirical mode decomposition (CEEMDAN) to extract time domain features and carried out two fast Fourier changes to extract deep frequency domain features. The results show that this method is effective and applicable in the actual fault diagnosis of wind turbine rolling bearings. The pulsation tracking network (PTN) [28,29] combined with the fast Fourier transform (FFT) can provide better visualization of draft tube pressure pulsations

and pulse signal decomposition, revealing the pulse frequency, amplitude, and phase. The method support is provided to reveal the influence law of the draft tube pressure pulsation. From the above-related research, it can be seen that although conventional analysis methods for pressure pulsation are effective, they lack intuitiveness. To determine the difference between two or more pressure pulsation signals, mode decomposition becomes crucial.

In engineering cases, the draft tube is generally arranged according to the civil structure, sometimes asymmetrically. This method does not fully consider the impact of fluid dynamics, which becomes a hidden danger in the operation process. On the basis of the above research, this paper carries out an analysis of the asymmetric layout of the draft tube and compares the left side tilt and the right side tilt. We hope to find out which direction is better for the arrangement of the draft tube. How to determine the specific placement direction of the draft tube is an unresolved issue. Based on computational fluid dynamics and Fourier's transformation, it can more clearly and directly reveal the law of pressure pulsation under the two situations. It is significant for the operation of the Francis turbine and the design of the draft tube for hydro turbines. This article conducts research based on practical engineering problems, and the innovative results provided can provide assistance and reference for other projects.

2. Francis Turbine Unit

2.1. Basic Parameters

Figure 1 shows the on-site Francis turbine unit with a three-dimensional model of the flow-passing components. This turbine unit is a prototype from the "Wanjiazhai Water Multi-purpose Dam Project" in Shanxi province, China. The top cover, main shaft, and runner are shown in the on-site pictures. The flow-passing components include the volute and stay vane for flow assembly, the guide vane for flow rate regulation, the runner for energy conversion, and the draft tube for flow guidance and pressure energy recovery. This turbine includes three cascades: the runner with 13 blades, the stay vane with 24 blades, and the guide vane also with 24 blades.

Figure 1. *Cont.*
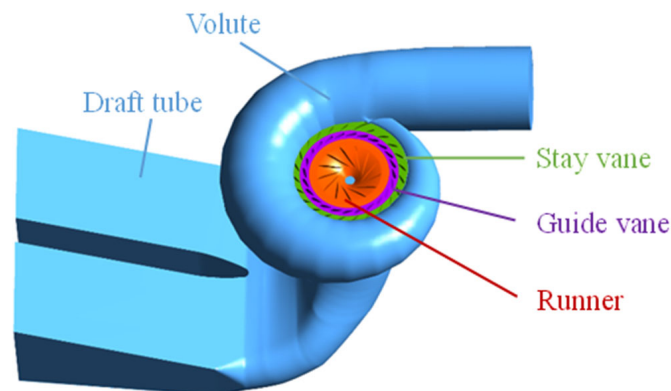
Figure 1. The on-site pictures and the flow-passing components of the Francis turbine.

The basic parameters of this turbine are listed as follows. The runner diameter D_{rn} is 5.80 m. The rated output power P_r is 183.7 MW. The rated flow rate Q_r is 301 m^3/s. The rated rotation speed n_r is 100 rpm. The rated water head H_r is 68.0 m. The maximum output power P_{max} is 204.1 MW. The turbine installation height H_{ins} is 895 m.

2.2. Asymmetric Arrangement of Draft Tube

In this study, the asymmetric layout of two types of draft tubes is considered, as shown in Figure 2. According to the rotation direction of the runner shown in Figure 2, the inlet of the volute is on the left side of the figure, and the water gradually rotates to the right. When the draft tube is asymmetrically arranged, the split buttress in the middle is not on the centerline of the rotation axis but has a certain offset. Left tilt (LT) is defined as the left deviation of the buttress and the draft tube flow passage. On the contrary, right tilt (RT) is defined as the deviation of the buttress and draft tube flow channel to the right as shown in the figure. From a hydrodynamic perspective, the two should not differ significantly due to the constant cross-sectional area of the flow. From the structural point of view, the draft tube of the left tilt occupies less additional space due to the large left area of the volute. On the contrary, the draft tube of the right tilt will occupy some additional space on the right side. In fact, because the rotating direction of the runner is fixed and the rotating flow is excited in the draft tube, the RT and LT arrangement of the draft tube will be different in pressure pulsation. This is the focused issue of this study.

(**a**) Left Tilt(LT)   (**b**) Right Tilt (RT)   (**c**) Left Tilt Draft
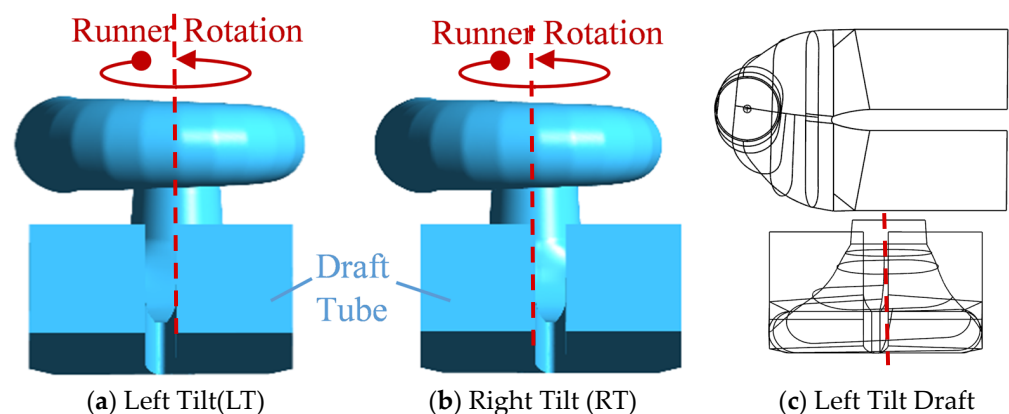
Figure 2. The left tile (LT) and right tilt (RT) of a draft tube of the Francis turbine.

3. Numerical Setup

3.1. Governing Equations

This study uses the Reynolds averaged Navier–Stokes equation to solve flow problems. Quantities are decomposed into averaged terms and pulsating terms [30]. The continuity equation and momentum equation can be written as follows:

$$\frac{\partial \overline{u_i}}{\partial x_i} = 0 \tag{1}$$

$$\rho \frac{\partial \overline{u_i}}{\partial t} + \rho \overline{u_j} \frac{\partial \overline{u_i}}{\partial x_j} = \frac{\partial}{\partial x_j}\left(-\overline{p}\delta_{ij} + 2\mu\overline{S_{ij}} - \rho\overline{u_i'u_j'}\right) \tag{2}$$

where t is time, ρ is density, u is velocity, μ is dynamic viscosity, x is coordinate component, and δ_{ij} is the Kroneker delta. The term named Reynold stress, represented as $\rho u_i'u_j'$, is not closed, so Boussinesq introduced the turbulence isotropy assumption, and it is developed to build the relationship between Reynolds stress and eddy viscosity μ_t [31]:

$$-\rho\overline{u_i'u_j'} = 2\mu_t\overline{S_{ij}} - \frac{2}{3}k\delta ij \tag{3}$$

where k is the turbulence kinetic energy, and S_{ij} is the mean rate of strain tensor:

$$\overline{S_{ij}} = \frac{1}{2}\left(\frac{\partial \overline{u_i}}{\partial x_j} + \frac{\partial \overline{u_j}}{\partial x_i}\right) \tag{4}$$

The eddy viscosity μ_t is connected to turbulence kinetic energy k and turbulence eddy frequency ω based on the experiment, and the shear stress transport (SST) model [32] is established by:

$$\frac{\partial(\rho k)}{\partial t} + \frac{\partial(\rho u_i k)}{\partial x_i} = P_k - \frac{\rho k^{3/2}}{l_{k-\omega}} + \frac{\partial}{\partial x_i}\left[(\mu + \sigma_k \mu_t)\frac{\partial k}{\partial x_i}\right] \tag{5}$$

$$\frac{\partial(\rho\omega)}{\partial t} + \frac{\partial(\rho u_i \omega)}{\partial x_i} = C_\omega P_\omega - \beta\rho\omega^2 + \frac{\partial}{\partial x_i}\left[(\mu_l + \sigma_\omega \mu_t)\frac{\partial\omega}{\partial x_i}\right] + 2(1-F_1)\frac{\rho\sigma_{\omega 2}}{\omega}\frac{\partial k}{\partial x_i}\frac{\partial\omega}{\partial x_i} \tag{6}$$

where P_k and P_ω are the production terms, F_1 is the coefficient of the production term, σ_k is the blending function, and σ_ω and β_k are model constants. $l_{k-\omega}$ is the turbulence scale, formulated as follows:

$$l_{k-\omega} = k^{1/2}\beta_k\omega \tag{7}$$

This model is good at both the strong shear flow and large pressure gradient. Applying the $k-\omega$ mode in the near-wall region overcomes the disadvantages of the $k-\varepsilon$ model series in capturing wall flow. With the mode of $k-\varepsilon$, the physical field gradient in the flow channel is described with great precision. Therefore, the SST model combines the advantages of both modes. This model provides a good solution for predicting flow problems in engineering cases.

3.2. CFD Setup with Monitoring Points

In this study, computational fluid dynamics (CFD) simulation is based on the commercial software ANSYS CFX 18.0. In total five components, i.e., volute, stay vane, runner, guide vane, and draft tube, are considered. Because the runner is rotating and other components are fixed, the multiple reference frame is used. Therefore, the fluid domain is also divided into five parts. General grid interfaces are given between each two parts. The volute inlet is set as the total pressure inlet boundary. The draft tube outlet is set as the static pressure outlet boundary. All walls are set as non-slip walls.

To evaluate the transient flow and pressure pulsation, a transient state simulation is conducted in this study. In total 10 runner revolutions are considered. In each revolution, 720 timesteps are considered. In each timestep, the iteration number is set as 5~20 and the convergence criterion is 1×10^{-5} for the residuals of both continuity and momentum equations. Figure 3 shows the monitoring points set in the draft tube. To investigate the pressure pulsation caused by vortex rope, P1~P4 are set as indicated. P1 and P2 are on the same higher plane and located on the left side and right side near the wall. P3 and P4 are on the same lower plane and located on the left side and right side also near the wall. In this CFD simulation work, we used a high-performance parallel computing workstation. The AMD EPYV 7813 64-core processor is used as the CPU with 128 threads. The frequency is 2.25 GHz. The memory of the workstation is 128 GB. For each transient simulation, the CPU time is approximately 82,800~90,000 s.
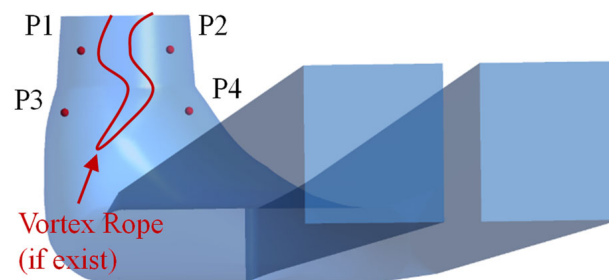
Figure 3. The CFD monitoring points in the draft tube of the Francis turbine.

3.3. Determination of Mesh

A reasonable mesh scheme is helpful to balance the computing cost and accuracy. ICEMCFD platform is used to generate three mesh schemes to conduct a check named "grid convergence index" (GCI) [33]. These three schemes are increased in spacing by 1.35. The efficiency η evaluated by CFD at rated conditions is used as the index. Figure 4 shows the check detail with a coarse mesh, a medium mesh, a fine mesh, and the Richardson extrapolated value. The GCI value of the coarse and medium grid is 3.91% and the GCI value of the medium and fine grid is 0.03%. The smaller the GCI value, the more accurate the simulation results. When the GCI value is less than 5%, the simulation result is acceptable. In order to balance the computational workload and accuracy, the medium scheme with 2.75 million mesh is chosen as the final mesh scheme as shown in Figure 5 and Table 1.
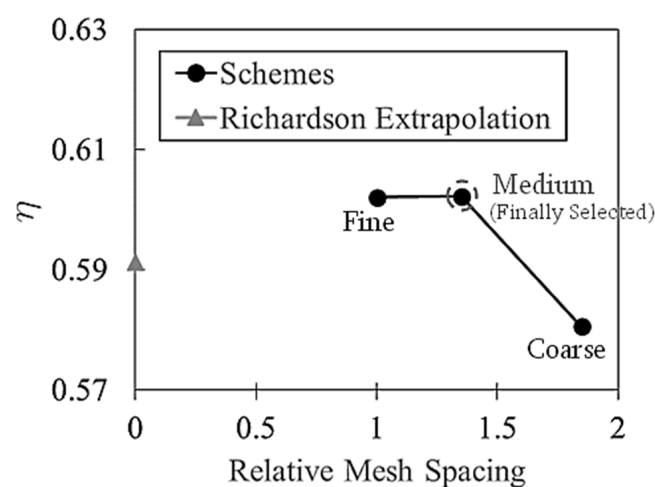
Figure 4. The mesh check based on GCI.
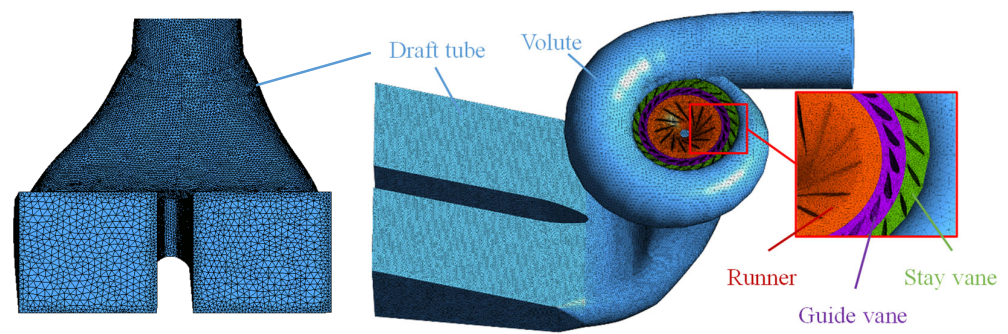
Figure 5. The schematic map of the finally chosen mesh.

Table 1. Mesh number details.

Component	Mesh Number	Range of y+	Average of y+
Volute	209,260	11–230	53
Stay vane	558,230	2–165	38
Guide vane	623,824	2–165	45
Runner	897,680	1.5–211	31
Draft tube	464,692	16–253	88
Total	2,753,686	—	—

4. Results of Performance Analysis

4.1. Efficiency Comparison

Figure 6 shows the operating curve of the water turbine. Its horizontal axis represents turbine power P. Its ordinate represents the water head H. The right side of the figure shows the power limit line, and the left side shows the area where the unit may operate. The optimal efficiency zone on the graph is close to the right. From the bottom right corner to the top left corner, instability gradually increases. Figure 6 shows three conditions for validation and verification. They are illustrated on the P-H map. The prototype Francis turbine's draft tube is left tilt. On the left side of the operation limitation line, with the decrease in power P and increase in head H, there are three regions defined as the "allowed region", "restricted region", and "prohibited region". The three chosen conditions are tagged by C_{alw}, C_{rst}, and C_{phb} with the unit rotation speed n_{11} of 77.85, 78.55, and 91.21 and the unit flow rate Q_{11} of 0.7864, 0.3678, and 0.3495. The definitions for n_{11} and Q_{11} are as follows:

$$n_{11} = \frac{nD_{rn}}{\sqrt{H}} \tag{8}$$

$$Q_{11} = \frac{Q}{D_{rn}^2 \sqrt{H}} \tag{9}$$

where n is the rotational speed and Q is the flow rate. Figure 7 shows the comparison of efficiency η between CFD and experimental data. At C_{alw}, the CFD efficiency is 91.05% for LT and 91.08% for RT, and the experimental efficiency is 90.51%. At C_{rst}, the CFD efficiency is 71.72% for LT and 71.69% for RT, and the experimental efficiency is 70.32%. At C_{phb}, the CFD efficiency is 55.25% for LT and 55.23% for RT, and the experimental efficiency is 52.88%. RT and LT show a good match on the performance. The CFD value shows a good prediction of unit performance and can be used for subsequent analysis.
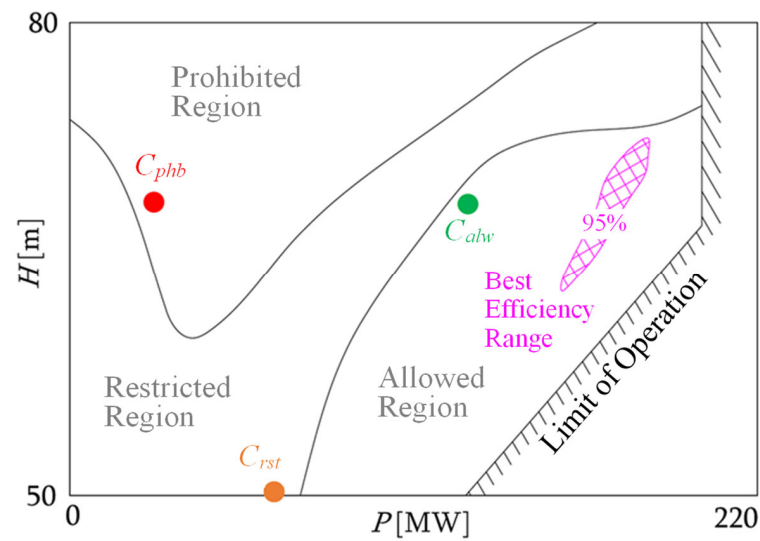
Figure 6. The operation characteristic *P-H* map.
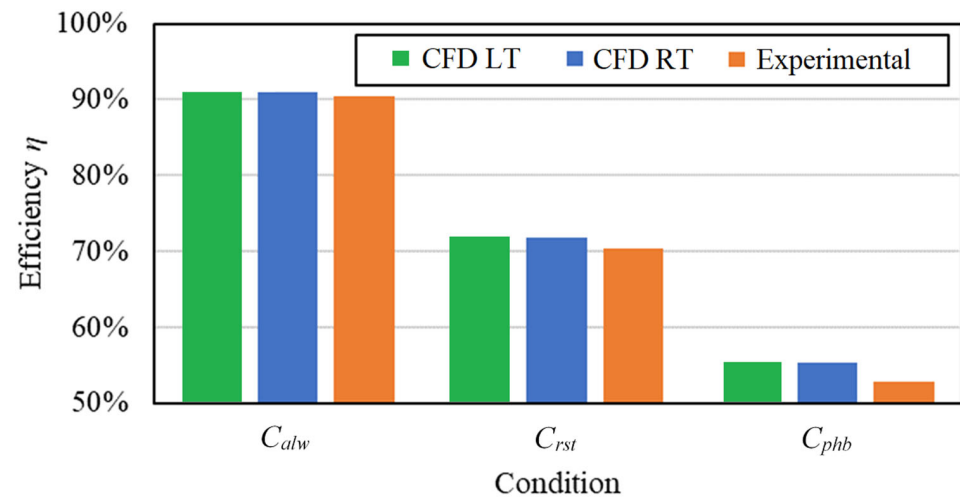
Figure 7. The comparison of efficiency for CFD-experiment verification and validation.

4.2. The Internal Flow Pattern

Figure 8 shows the flow inside the Francis turbine, using colored streamlines to represent the velocity and direction of the flow. It can be seen that the performance of LT and RT in internal flow is very similar, and there is almost no difference. This is also why the performance of the two is so close. At the C_{alw} point in the allowed region, the flow is relatively stable and the streamline is smooth. Velocity in runner is uniform and up to about 20 m/s. At the C_{rst} point in the restricted region, the velocity in the runner increases to a maximum of about 38 m/s and the distribution of velocity becomes non-uniform. The flow in the draft tube develops many vortexes. The vortical flow dominates the component downstream to the runner and seems out of control. At the C_{phb} point in the prohibited region, the velocity in the runner is still relatively high (maximum value is about 35 m/s). The vortical flow in the draft tube further intensifies. In comparison, the flow status is relatively worse in prohibited and restricted operating regions.

(**a**) Condition C_{alw}

(**b**) Condition C_{rst}

(**c**) Condition C_{phb}
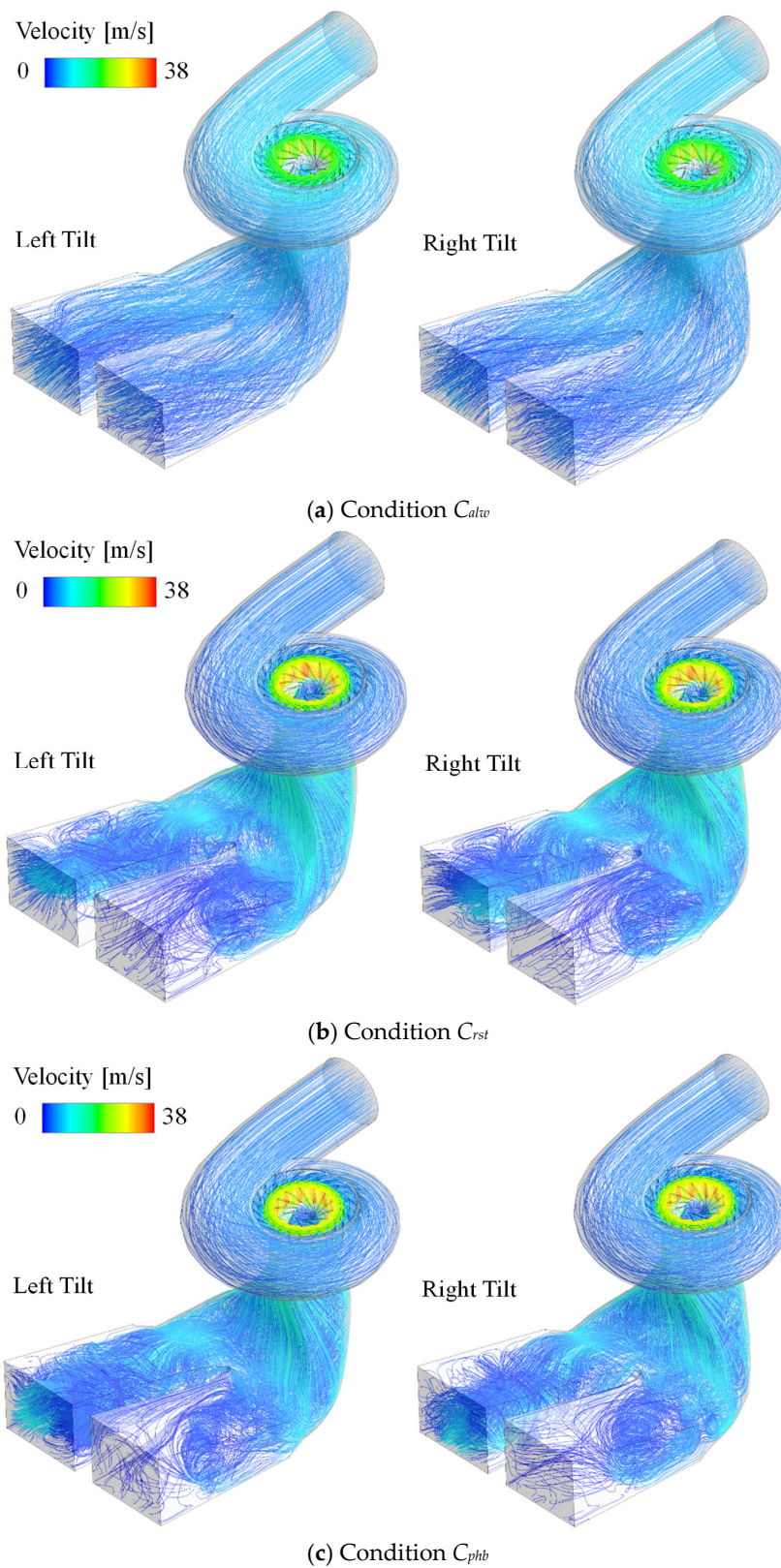
Figure 8. Internal flow pattern in Francis turbine.

5. Results of Pressure Pulsation Analysis

Variational modal decomposition (VMD) is an adaptive, completely non-recursive method for modal decomposition and signal processing, which can decompose pressure pulsation signals into a set of IMF components with different frequencies. Based on

the points P1~P4 shown in Figure 3, analyses are conducted using the variational mode decomposition (VMD) method, which is used to decompose the pressure pulsation of four monitoring points under the conditions of the left and right tilts of the draft tube of the turbine. This is the first time that the VMD method has been introduced into the study of pressure pulsation in the Francis turbine, which provides assistance in clearly extracting signal features and obtaining clearer results. The time domain diagram of each component and its corresponding frequency domain diagram obtained from the decomposition are shown in Figures 9–12. Several intrinsic mode functions (IMFs) are indicated for a better analysis.
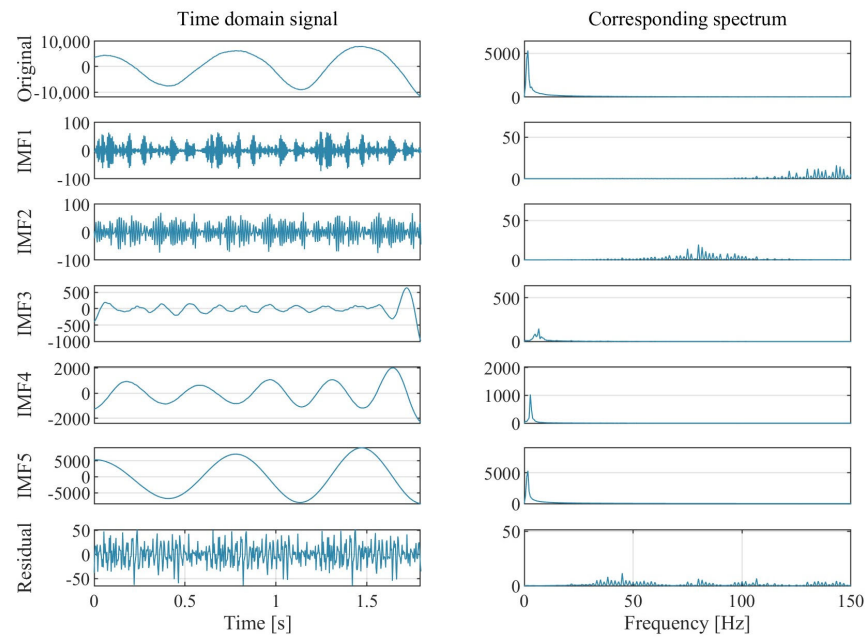
(**a**) Left Tilt
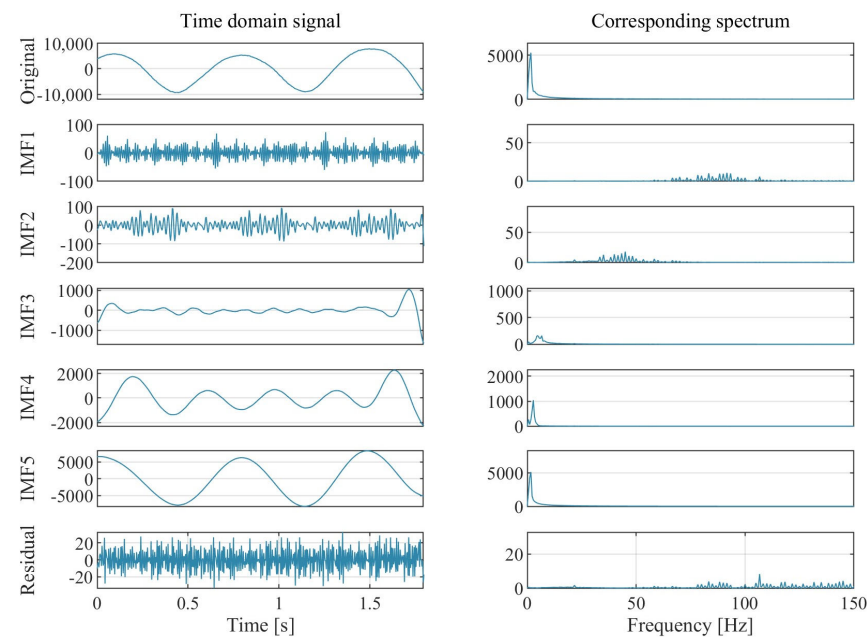
(**b**) Right Tilt

Figure 9. Time domain diagram and corresponding spectrum of P1 pressure pulsation signal based on VMD decomposition under different operating conditions.
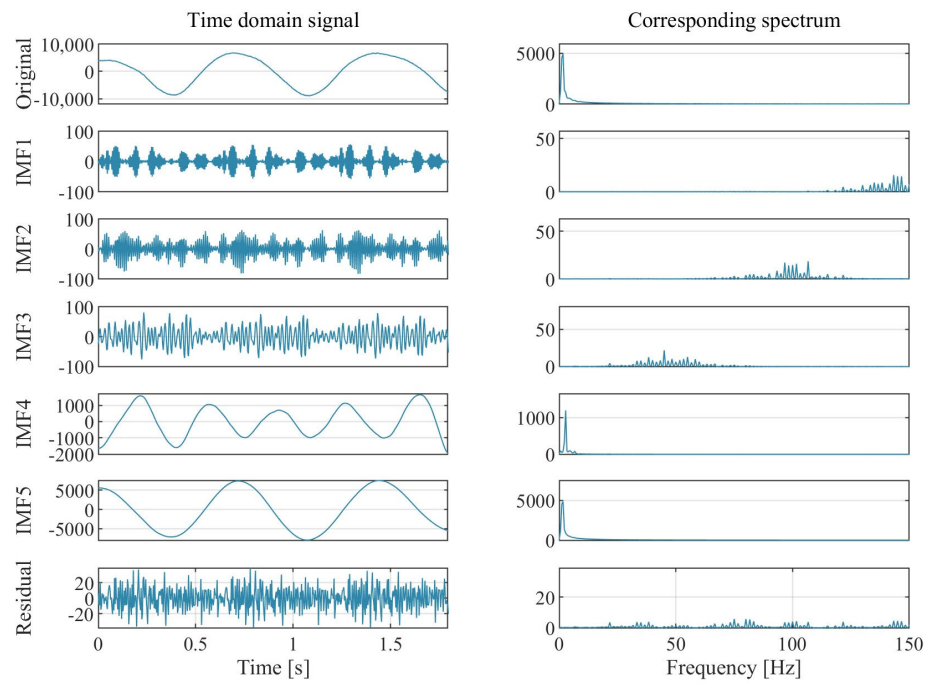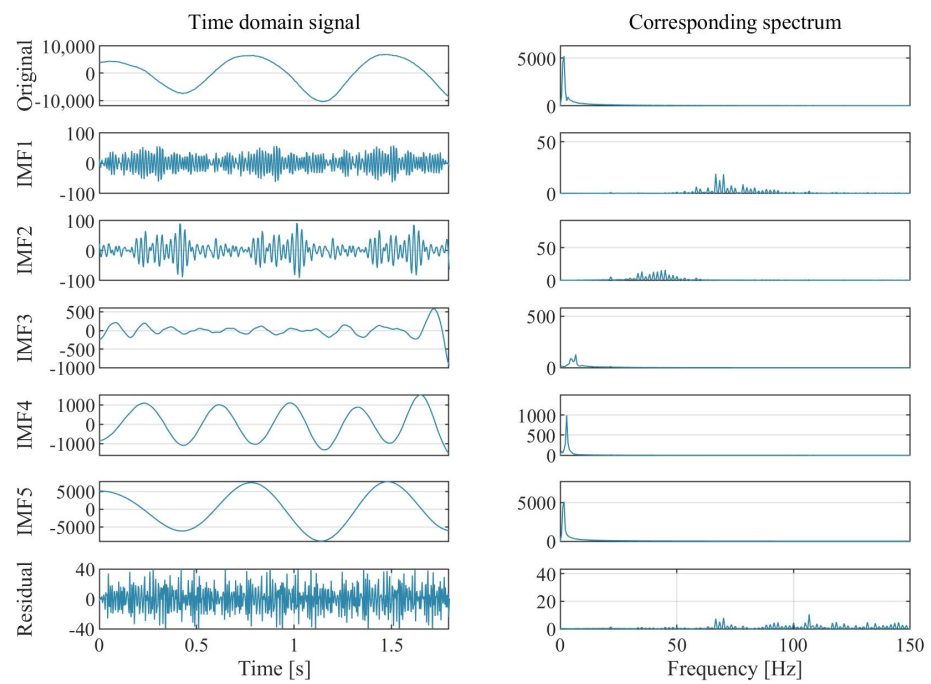
(**a**) Left Tilt

(**b**) Right Tilt

Figure 10. Time domain diagram and corresponding spectrum of P2 pressure pulsation signal based on VMD decomposition under different operating conditions.
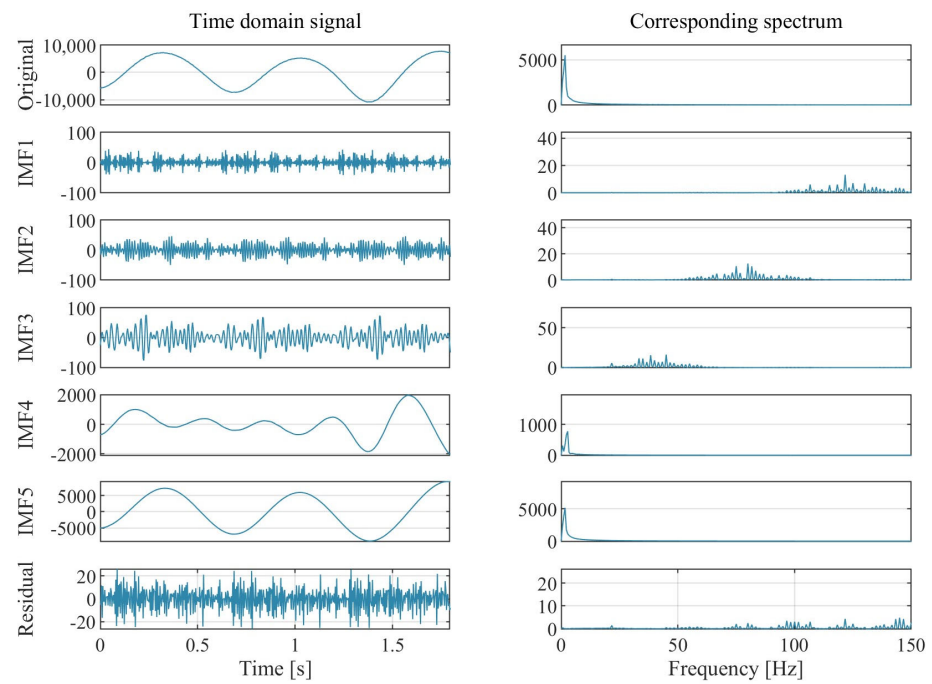
(**a**) Left Tilt
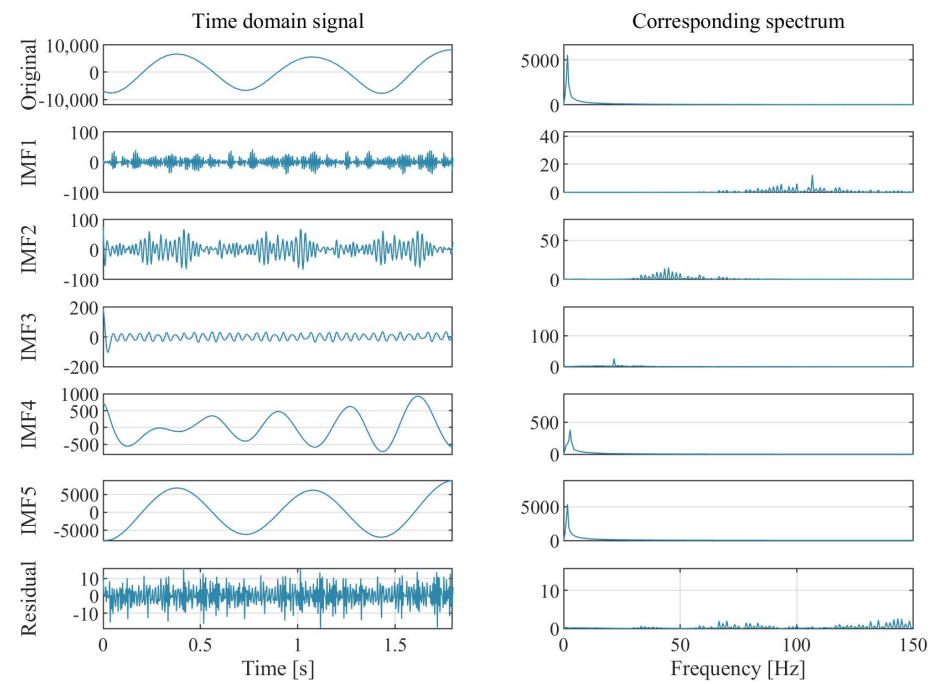
(**b**) Right Tilt

Figure 11. Time domain diagram and corresponding spectrum of P3 pressure pulsation signal based on VMD decomposition under different operating conditions.
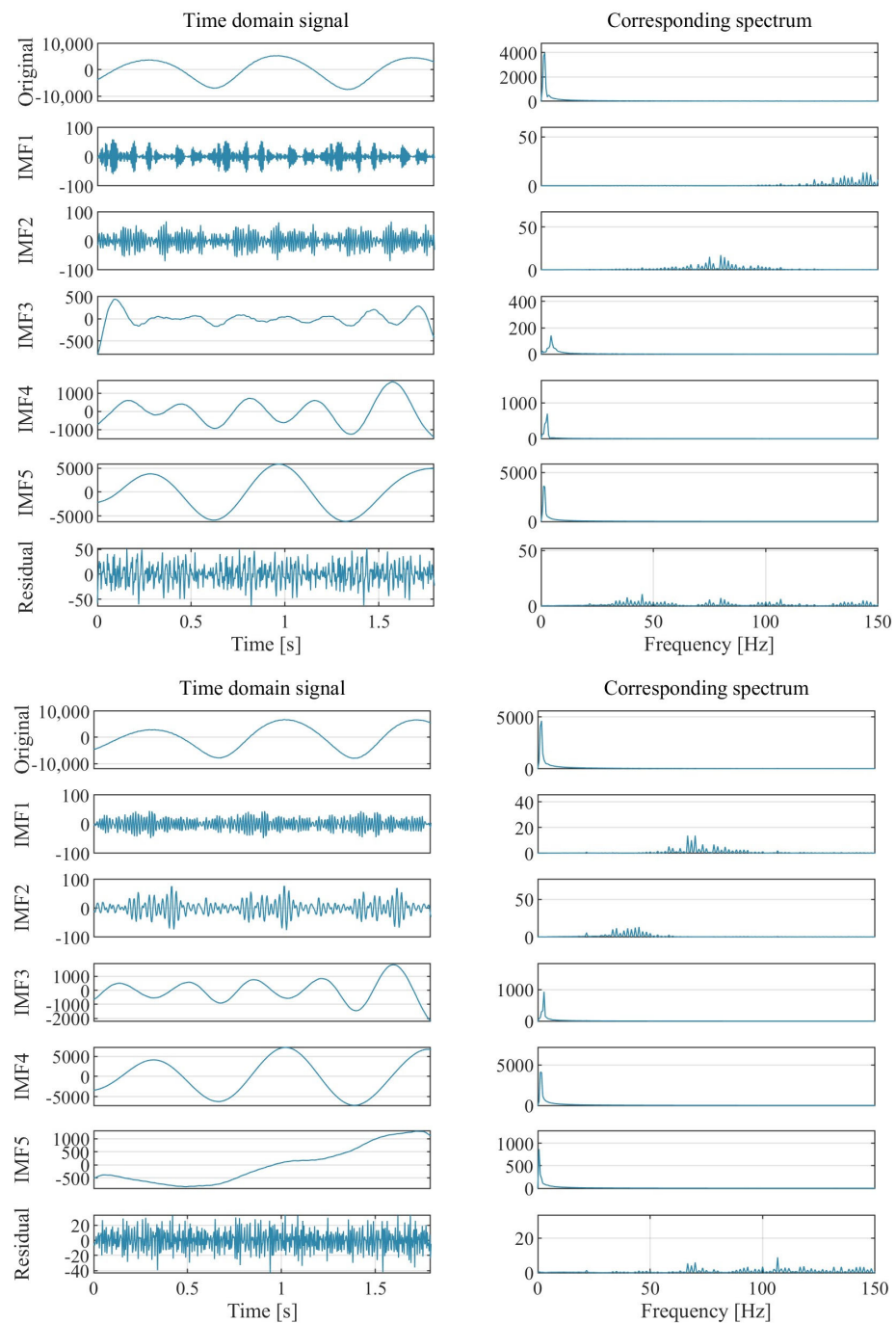
(**b**) Right Tilt

Figure 12. Time domain diagram and corresponding spectrum of P4 pressure pulsation signal based on VMD decomposition under different operating conditions.

5.1. Analysis of Time Domain and Frequency Domain

Figure 9 shows the time domain diagrams and corresponding frequency spectra of each component obtained by decomposing the pressure pulsation signal of the P1 monitoring point using VMD under different working conditions. It can be seen from the figure that the frequency domain diagram and time domain diagram of each component obtained by VMD decomposition are basically similar under the conditions of the left and right tilts of the draft tube. There is only one wave peak in the frequency domain diagram of IMF4 and IMF5 components. When the draft tube tilts to the left, the peak value of the frequency

domain diagram of IMF5 is 5314 Pa, the peak frequency is the rotating frequency of the runner f_r (1.67 Hz), the peak value of the frequency domain diagram of IMF4 is 1032 Pa, and the peak frequency is 2.78 Hz. When the draft tube tilts to the right, the peak value of the frequency domain diagram of IMF5 is 5126 Pa, the peak frequency is 1.67 Hz, the peak value of the frequency domain diagram of IMF4 is 1041 Pa, and the peak frequency is 2.78 Hz. It can be seen that the pressure pulsation of the draft tube is mainly affected by the rotating frequency of runner f_r, while the left and right tilts of the draft tube have little influence on the IMF1 and IMF2 components. The frequency domain diagram of IMF1–IMF3 is composed of multiple high-frequency signals with low amplitude. When the draft tube tilts to the left, the center frequencies of IMF1–IMF3 components are 137.1 Hz, 81.36 Hz, and 6.24 Hz, respectively. When the draft tube tilts to the right, the center frequencies of IMF1–IMF3 components are 87.7 Hz, 42.3 Hz, and 5.51 Hz, respectively. Different draft tube tilt conditions have a greater impact on the center frequency of high-frequency components. When the draft tube tilts to the left, the center frequency of the IMF1–IMF3 component of pressure pulsation at the P1 monitoring point is significantly greater than that of the draft tube tilts to the right.

Figure 10 shows the time domain diagrams and corresponding frequency spectra of each component obtained by decomposing the pressure pulsation signal of the P2 monitoring point using VMD under different working conditions. When the draft tube tilts to the left, the amplitude of the IMF5 component is 4851 Pa, and the amplitude of the IMF4 component is 1196 Pa. When the draft tube tilts to the right, the amplitude of the IMF5 component is 5126 Pa, and the amplitude of the IMF4 component is 991 Pa. Compared with the right tilt of the draft tube, the left tilt of the draft tube can reduce the pressure pulsation at monitoring point P2 to a certain extent, which is of great significance to the stable operation of the unit. The P1 and P2 monitoring points are located on both symmetrical sides, and the difference in pressure pulsation between them may be related to the asymmetric volute. At the P2 monitoring point, the center frequencies of IMF1–IMF3 components are 141.41 Hz, 99.89 Hz, and 46.85 Hz, respectively, when the draft tube tilts to the left. When the draft tube tilts to the right, the center frequencies of IMF1–IMF3 components are 78.28 Hz, 42.06 Hz, and 5.78 Hz, respectively. When the draft tube tilts to the left, the center frequency of IMF1–IMF3 components at the P2 monitoring point is significantly different from that at the P1 monitoring point. When the draft tube tilts to the right, the center frequencies of the P1 and P2 monitoring points are basically the same, which indicates that the left tilt of the draft tube has a greater impact on the internal pressure pulsation of the draft tube.

Figure 11 shows the time domain diagrams and corresponding frequency spectra of each component obtained by decomposing the pressure pulsation signals of P3 monitoring points using VMD under different operating conditions. When the draft tube tilts to the left, the amplitude of the IMF5 component is 5193 Pa, and the amplitude of the IMF4 component is 782 Pa. When the draft tube tilts to the right, the amplitude of the IMF5 component is 5370 Pa, and the amplitude of the IMF4 component is 379 Pa. Similar to the P1 monitoring point, different draft tube tilt conditions have little impact on the amplitude of pressure pulsation at the P3 monitoring point. Under the two conditions, the difference in pressure pulsation amplitude is only 3.3%. At the P3 monitoring point, when the draft tube tilts to the left, the center frequencies of IMF1–IMF3 components are 139.33 Hz, 93.67 Hz, and 41.29 Hz, respectively. When the draft tube tilts to the right, the center frequencies of IMF1–IMF3 components are 102.43 Hz, 45.16 Hz, and 20.28 Hz, respectively. When the draft tube tilts to the left, the center frequency of the IMF1–IMF3 component is significantly higher than that of the draft tube tilts to the right, and the center frequencies of the IMF4 and IMF5 components are basically the same, which is basically the same as the impact of draft tube tilt on the center frequency of the P1 monitoring point.

Figure 12 shows the time domain diagrams and corresponding frequency spectra of each component obtained by decomposing the pressure pulsation signals of P4 monitoring points using VMD under different operating conditions. When the draft tube tilts to the

left, the amplitude of the IMF5 component is 3626 Pa, and the amplitude of the IMF4 component is 695 Pa. When the draft tube tilts to the right, the amplitude of the IMF5 component is 871 Pa, and the amplitude of the IMF4 component is 4119 Pa. Different from other monitoring points, the amplitude–frequency of the IMF5 component at the P4 monitoring point is 0.56 Hz when draft tube tilts to the right, and the amplitude–frequency of IMF4 is runner frequency f_r. Compared with the draft tube tilting to the right, the pressure pulsation amplitude of the draft tube tilting to the left can be reduced by 11.9%. When the draft tube is tilted to the left, the center frequencies of IMF1–IMF3 components are 141.41 Hz, 99.89 Hz, and 46.85 Hz, respectively. When the draft tube tilts to the right, the center frequencies of IMF1–IMF3 components are 78.28 Hz, 42.06 Hz, and 5.78 Hz, respectively. At this point, there is a significant difference in the center frequency of the pressure pulsation component between the P4 monitoring point and the P3 monitoring point under both operating conditions. This shows that as the monitoring point moves downstream of the draft tube, the larger the draft tube tilt, the greater the impact of the tilt on the draft tube pressure pulsation, and the more significant the impact of the left tilt of the draft tube on reducing the amplitude of pressure pulsation.

5.2. The Law of Pressure Pulsation

Table 2 summarizes the law of pressure pulsation of all four monitoring points with the comparison between left tilt and right tilt. Overall, there are seven characteristic frequency bands, including approximately 140 Hz, 80–90 Hz, 40–46 Hz, 5.5–6.5 Hz, 2.5–3 Hz, f_r (1.67 Hz), and <1 Hz. The frequency value of the same mode of left tilt is higher than that of the right tilt. In addition, the intensity of the runner frequency f_r is very important, as analyzed in Figure 13. On P1, the amplitudes of LT and RT are similar. On P2, RT has a higher amplitude of f_r than that of LT. On P3, RT has a slightly higher amplitude of f_r than that of LT. On P4, RT has a higher amplitude of f_r than that of LT and the difference becomes bigger. Generally, the right tilt draft tube may trigger higher pulsation of the pressure field.

Table 2. IMFs of all four monitoring points.

	Left Tilt				Right Tilt			
	P1	**P2**	**P3**	**P4**	**P1**	**P2**	**P3**	**P4**
IMF1 (Hz)	137.10	141.41	139.33	138.67	87.70	78.28	102.43	71.15
IMF2 (Hz)	81.36	99.89	93.67	78.72	42.30	42.06	45.16	40.25
IMF3 (Hz)	6.24	46.85	41.29	4.67	5.51	5.78	20.28	2.58
IMF4 (Hz)	2.89	2.77	2.27	2.35	2.60	2.80	2.75	1.34
IMF5 (Hz)	1.41	1.38	1.33	1.33	1.35	1.40	1.37	0.34
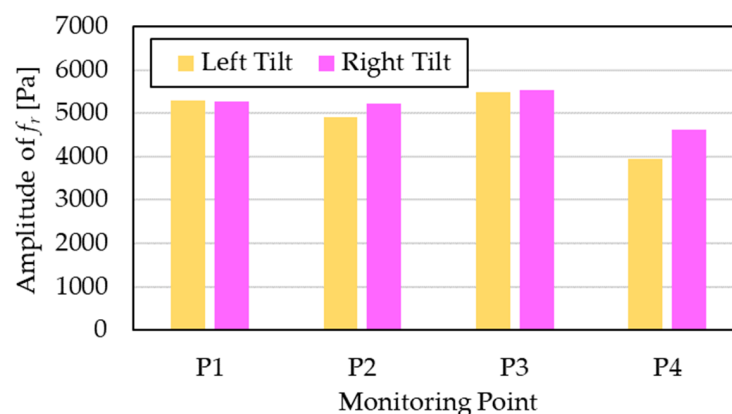
Figure 13. Pulsation amplitude of runner frequency f_r on all four monitoring points of the left tilt and right tilt of the draft tube.

6. Conclusions

This study focuses on the influence of the asymmetric arrangement (tilt) direction of a draft tube on the pressure pulsation of a Francis turbine, and conclusions can be drawn as follows:

(1) Left-tilt arrangement and right-tilt arrangement of the draft tube have little impact on the unit performance of the Francis turbine. By comparing the CFD calculation and analysis results with the prototype measurement results, it can be found that the direction of the asymmetric arrangement of the draft tube has little effect on the efficiency. As long as the cross-sectional area remains unchanged, the variation in total pressure remains unchanged, and the impact of left and right tilts on different working conditions is relatively small, typically less than 1% on efficiency. Therefore, from the perspective of hydraulic performance, the tilt direction of the draft tube can be left or right.

(2) From the internal flow, it can be seen that there are significant differences in the flow inside the unit under different operating conditions. In the allowed region with higher efficiency, the flow smoothness is relatively high, and there are almost no obvious vortices or other forms of adverse flow patterns visible. In restricted and prohibited regions, the velocity distribution will be uneven, and the local velocity may be very high. Flow in the draft tube has also become chaotic, mainly with large-scale strong rotating flow. Judging from the characteristics of the flow direction, both the left-tilt and right-tilt draft tubes are acceptable. The impact of the left-tilt arrangement and right-tilt arrangement is still not significant, and the difference is almost invisible.

(3) Based on the mode decomposition of the pressure fluctuation signal by VMD, it can be seen that different arrangement directions of the draft tube will have some effects on the flow. Overall, the frequency characteristics of the two are relatively similar with no huge differences. However, the dominant mode of the left tilt corresponds to a higher frequency, while the right tilt corresponds to a lower frequency. In addition, in terms of the amplitude of the important runner frequency f_r, the value corresponding to the right tilt is slightly higher than that of the left tilt. From a hydrodynamic perspective, the geometric features of flow-passing components that are more adaptable to flow are more acceptable. If the left tilt is used, the fluctuation in the flow field may be more stable due to the same arrangement direction of the draft tube and volute.

In general, this study gives a hydrodynamic reference of the design of draft tube of Francis turbines and can be applied to other cases of hydro turbines. The innovation of this article lies in relying on real engineering cases to conduct in-depth and detailed analyses of small problems, providing great assistance for the promotion of the results. In the future, we will carry out construction and renovation of the tailwater pipes of the power plant and compare the impact of different inclined tailwater pipes on the stability of the unit during actual operation. In addition, through numerical simulations, we will also compare the effects of other units and different degrees of inclination of the draft tube, deepen our research, and provide more support for the design of hydropower stations.

Data Availability Statement: Data are contained within the article.

References

1. Kose, F.; Kaya, M.N. Analysis on meeting the electric energy demand of an active plant with a wind-hydro hybrid power station in Konya, Turkey: Konya water treatment plant. *Renew. Energy* **2013**, *55*, 196–201. [CrossRef]
2. Wu, Y.; Zhang, J.; Yuan, J.; Geng, S.; Zhang, H. Study of decision framework of offshore wind power station site selection based on ELECTRE-III under intuitionistic fuzzy environment: A case of China. *Energy Convers. Manag.* **2016**, *113*, 66–81. [CrossRef]
3. Tao, R.; Lu, J.; Jin, F.; Hu, Z.; Zhu, D.; Luo, Y. Evaluation of the rotor eccentricity added radial force of oscillating water column. *Ocean Eng.* **2023**, *276*, 114222. [CrossRef]
4. Dong, J.; Feng, T.-T.; Yang, Y.-S.; Ma, Y. Macro-site selection of wind/solar hybrid power station based on ELECTRE-II. *Renew. Sustain. Energy Rev.* **2014**, *35*, 194–204.
5. Jafari, B.; Seddiq, M.; Mirsalim, S.M. Impacts of diesel injection timing and syngas fuel composition in a heavy-duty RCCI engine. *Energy Convers. Manag.* **2021**, *247*, 114759. [CrossRef]
6. Ping, X.; Yang, F.; Zhang, H.; Zhang, J.; Xing, C.; Yan, Y.; Yang, A.; Wang, Y. Information theory-based dynamic feature capture and global multi-objective optimization approach for organic Rankine cycle (ORC) considering road environment. *Appl. Energy* **2023**, *348*, 121569. [CrossRef]
7. Jafari, B.; Seddiq, M.; Mirsalim, S.M. Assessment of the impacts of combustion chamber bowl geometry and injection timing on a reactivity controlled compression ignition engine at low and high load conditions. *Int. J. Engine Res.* **2021**, *22*, 2852–2868. [CrossRef]
8. Zhou, M.; Ye, Q.; Liu, Z. Climate impacts on hydro-power development in China. *Bot. Mar.* **2005**, *19*, 1–4.
9. Pereira, J.G.; Vagnoni, E.; Favrel, A.; Landry, C.; Alligne, S.; Nicolet, C.; Avellan, F. Prediction of unstable full load conditions in a Francis turbine prototype. *Mech. Syst. Signal Process.* **2022**, *169*, 108666. [CrossRef]
10. Kalantar, M.; Mousavi, S.M.G. Dynamic behavior of a stand-alone hybrid power generation system of wind turbine, microturbine, solar array and battery storage. *Appl. Energy* **2010**, *87*, 3051–3064. [CrossRef]
11. Zhu, D.; Tao, R.; Xiao, R.; Pan, L. Solving the runner blade crack problem for a Francis hydro-turbine operating under condition-complexity. *Renew. Energy* **2020**, *149*, 298–320. [CrossRef]
12. Li, P.; Xiao, R.; Tao, R. Study of vortex rope based on flow energy dissipation and vortex identification. *Renew. Energy* **2022**, *198*, 1065–1081. [CrossRef]
13. Zhu, D.; Yan, W.; Guang, W.; Wang, Z.; Tao, R. Influence of guide vane opening on the runaway stability of a pump-turbine used for hydropower and ocean power. *J. Mar. Sci. Eng.* **2023**, *11*, 1218. [CrossRef]
14. Tamura, Y.; Tani, K.; Okamoto, N. Experimental and numerical investigation of unsteady behavior of cavitating vortices in draft tube of low specific speed Francis turbine. *IOP Conf. Ser. Earth Environ. Sci.* **2014**, *22*, 032011. [CrossRef]
15. Arthur, F.; Muller, A.; Landry, C.; Yamamoto, K.; Avellan, F. LDV survey of cavitation and resonance effect on the precessing vortex rope dynamics in the draft tube of Francis turbines. *Exp. Fluids* **2016**, *57*, 168.
16. Zhang, J.; Appiah, D.; Zhang, F.; Yuan, S.; Gu, Y.; Asomani, S.N. Experimental and numerical investigations on pressure pulsation in a pump mode operation of a pump as turbine. *Energy Sci. Eng.* **2019**, *7*, 1264–1279. [CrossRef]
17. Bosioc, A.I.; Susan-Resiga, R.; Muntean, S.; Tanasa, C. Unsteady pressure analysis of a swirling flow with vortex rope and axial water injection in a discharge cone. *J. Fluids Eng.* **2012**, *134*, 669–679. [CrossRef]
18. Geng, C.; Li, Y.; Tsujimoto, Y.; Nishi, M.; Luo, X. Pressure oscillations with ultra-low frequency induced by vortical flow inside Francis turbine draft tubes. *Sustain. Energy Technol. Assess.* **2022**, *51*, 101908. [CrossRef]
19. Liu, S.; Shao, Q.; Yang, J.; Wu, Y.; Dai, J. Unsteady turbulent simulation of Three Gorges hydraulic turbine and analysis of pressure in the whole passage. *J. Hydroelectr. Eng.* **2004**, *23*, 97–101.
20. Liao, W.; Ji, J.; Lu, P.; Luo, X. Unsteady flow analysis of francis turbine. *Chin. J. Mech. Eng.* **2009**, *45*, 134–140. [CrossRef]
21. Zhang, Y.; Liu, S.; Wu, Y. Detailed simulation and analysis of pressure pulsation in Francis turbine. *J. Hydroelectr. Eng.* **2009**, *28*, 183–186.
22. Pasche, S.F.; Gallaire, F.; Avellan, F. Origin of the synchronous pressure pulsations in the draft tube of Francis turbines operating at part load conditions. *J. Fluids Struct.* **2019**, *86*, 13–33. [CrossRef]
23. Kim, H.H.; Rakibuzzaman, M.; Kim, K.; Suh, S.-H. Flow and fast fourier transform analyses for tip clearance effect in an operating kaplan turbine. *Energies* **2019**, *12*, 264. [CrossRef]

24. Wu, Y.; Guang, W.; Tao, R.; Liu, J. Dynamic mode structure analysis of the near-wake region of a Savonius-type hydrokinetic turbine. *Ocean Eng.* **2023**, *282*, 114965. [CrossRef]
25. Tian, L.; Wu, J. Fault diagnosis and analysis of submersible sewage pump based on zoom-fft. *Mach. Des. Res.* **2018**, *34*, 171–174.
26. Wang, W.; Tai, G.; Shen, J. Experimental investigation on pressure pulsation characteristics of a mixed-flow pump as turbine at turbine and runaway conditions. *J. Energy Storage* **2022**, *55 Pt C*, 105562. [CrossRef]
27. Tang, Z.; Wang, M.; Ouyang, T.; Fei, C. A wind turbine bearing fault diagnosis method based on fused depth features in time–frequency domain. *Energy Rep.* **2022**, *8*, 12727–12739. [CrossRef]
28. Jin, F.; Tao, R.; Lu, Z.; Xiao, R. A spatially distributed network for tracking the pulsation signal of flow field based on CFD simulation: Method and a case study. *Fractal Fract.* **2021**, *5*, 181. [CrossRef]
29. Lu, Z.; Tao, R.; Jin, F.; Li, P.; Xiao, R.; Liu, W. The Temporal-Spatial Features of Pressure Pulsation in the Diffusers of a Large-Scale Vaned-Voluted Centrifugal Pump. *Machines* **2021**, *9*, 266. [CrossRef]
30. Pope, S.B. *Turbulent Flows*; Cambridge University Press: Cambridge, UK, 2000.
31. Terentiev, L. *The Turbulence Closure Model Based on Linear Anisotropy Invariant Analysis*; VDM Verlag: Saarbrucken, Germany, 2008.
32. Menter, F.R. Two-Equation Eddy-Viscosity Turbulence Models for Engineering Applications. *AIAA J.* **1994**, *32*, 1598–1605. [CrossRef]
33. Celik, I.B.; Ghia, U.; Roache, P.J.; Freitas, C.J.; Coloman, H.; Raad, P.E. Procedure for estimation and reporting of uncertainty due to discretization in CFD applications. *J. Fluids Eng.* **2008**, *130*, 78001.